Iranian Journal of Numerical Analysis and Optimization
Vol. 16, No. 1, 2026, pp 77–101
https://doi.org/10.22067/ijnao.2025.94700.1692
https://ijnao.um.ac.ir/

Research Article

Fractional-order modeling and numerical analysis of double intermediate enzymatic reaction model using generalized Euler method

B. Koushick, N. Anbazhagan, R. Vignesh Raju, N. Jeeva*

Abstract

This study investigates the fractional modeling of a double intermediate enzymatic reaction model using the Caputo derivative. A system of nonlinear fractional differential equations is

*Corresponding author

Received 31 July 2025; revised 31 October 2025; accepted 15 November 2025

B. Koushick
Department of Mathematics, Alagappa University, Karaikudi 630003, Tamil Nadu, India. e-mail: koushick@alagappauniversity.ac.in

N. Anbazhagan
Department of Mathematics, Alagappa University, Karaikudi 630003, Tamil Nadu, India. e-mail: anbazhagann@alagappauniversity.ac.in

R. Vignesh Raju
PG & Research Department of Mathematics, Vidhyaa Giri College of Arts and Science, Puduvayal 630108, Tamil Nadu, India. e-mail: vignesh1325@gmail.com

N. Jeeva
Department of Mathematics, K.S.Rangasamy College of Technology, Tiruchengode 637215, Namakkal (Dt.), Tamil Nadu, India
Centre for Research and Development, K.S.Rangasamy College of Technology, Tiruchengode 637215, Namakkal (Dt.), Tamil Nadu, India e-mail: jeevapirc2405@gmail.com

How to cite this article
Koushick, B., Anbazhagan, N., Vignesh Raju, R. and Jeeva, N., Fractional-order modeling and numerical analysis of double intermediate enzymatic reaction model using generalized Euler method. *Iran. J. Numer. Anal. Optim.*, 2026; 16(1): 77-101. https://doi.org/10.22067/ijnao.2025.94700.1692

formulated in dimensionless form to capture the complex dynamics of intermediate enzymes. The properties of the model are explored using key theorems related to fractional calculus. The generalized Euler method is employed to obtain numerical solutions for various fractional orders, highlighting the memory-dependent behavior of the system. The numerical simulations are consistent with theoretical expectations, confirming the validity and effectiveness of the proposed method. Various dimensionless parameters are systematically altered, and the corresponding system responses are captured using two-dimensional plots and surface visualizations in MATLAB®. The simulation results highlight that variations in these parameters significantly influence the transient and steady-state dynamics, illustrating their biochemical relevance and the utility of the fractional-order model in capturing such sensitivities.

AMS subject classifications (2020): Primary 34A34; Secondary 34E10, 65L05.

Keywords: Enzyme reaction model; Dimensionless formation; Fractional derivative; Extended Euler method; Numerical simulation

1 Introduction

Enzymes, which are proteins composed of amino acids, play a vital role in facilitating chemical transformations in various fields, including biochemistry, the food industry, and biological systems. As biological catalysts, enzymes accelerate the rate of chemical reactions without being consumed or being permanently altered. Each enzyme is highly specific and promotes a reaction with a specific substrate. During the catalytic process, the enzyme binds to the substrate and often undergoes a temporary change in its shape to facilitate the reaction. This interaction illustrates the precise relationship between the enzymes and their substrates. In enzymology, pre-steady-state kinetics focuses on the initial phase of a reaction prior to the formation of products or intermediates, offering insights into the early molecular interactions between enzymes and substrates [21, 13].

Mathematical models are essential tools for understanding complex dynamic systems, allowing researchers to simulate and analyze the interactions between various components. These models help predict the system behavior, optimize conditions, and explore the effects of various factors on dynamic processes. Analytical solutions provide approximate expressions that describe the temporal evolution of these interactions, and offer insights into the underlying mechanisms without relying on numerical approximations. By applying advanced techniques like the optimal homotopy analysis method, homotopy perturbation method, Taylor series method, Abkari–Ganji

method, and Pade approximation method, researchers can capture detailed system behavior, especially during early transient phases [4, 9, 10, 19, 18, 16, 17].

Several studies have demonstrated the power of mathematical modeling to advance our understanding of enzyme kinetics. For instance, Murrary [20] proposed a novel method to solve the time-dependent Michaelis–Menten enzymatic reaction by reducing the system to a single nonlinear ordinary differential equation and applying the optimal homotopy analysis method to obtain accurate and efficient analytical solutions. M.S. Ibrahim et al. [8] utilized the variational iteration method to address nonlinear enzyme reaction systems, showcasing its effectiveness in capturing the complex dynamics of enzymatic processes. Sharmila, Praveen, and Rajendran [27] conducted an in-depth mathematical study on enzyme-catalyzed reactions, shedding light on the impact of kinetic parameters through rigorous analysis. Similarly, previous work [28] has been focused on deriving exact solutions to nonlinear boundary value problems related to enzyme-substrate interactions, highlighting the significance of analytical methods in understanding biochemical reaction mechanisms. Collectively, these contributions underscore the essential role of mathematical approaches in the modeling, analysis, and optimization of enzyme-driven processes.

Frenzen [5] introduced an innovative application of the quasi-steady state assumption (QSSA) to a two-step enzymatic reaction model, expanding its applicability by allowing the initial enzyme-to-substrate concentration ratio to take any positive value, rather than being limited to small ratios. This further reveals that maintaining a constant enzyme-to-substrate ratio while reducing the initial substrate concentration enables the fulfillment of QSSA validity conditions, thereby broadening its practical utility in enzymatic kinetics. Recently, the study in [23] theoretically investigated the pre-steady-state dynamics of nonlinear enzymatic reactions that involve two intermediate complexes. Approximate analytical solutions for the concentrations of the substrate, first enzyme-substrate complex, and second complex were derived using homotopy perturbation and Taylor series. The accuracy of these analytical solutions was validated by comparing them with numerical simulation results. Saad, Abdo, and Hamanah [24] investigated the existence and controllability of multi-term fractional coupled systems using the generalized $(\psi\ ,\ \omega)$-Caputo-Fabrizio operator. Alqhtani, Sadek, and Saad [2] introduced the Mittag-Leffler–Caputo–Fabrizio fractional derivative and presented a corresponding numerical approach for its implementation.

Recent studies have explored advanced modeling approaches to better understand complex biochemical dynamics using fractional calculus. These studies include the development and simulation of nonlinear fractional-order biochemical reaction models and application of fractal–fractional derivatives with different kernels. Researchers have also investigated high-performance computational techniques for analyzing reversible two-step reactions with time-fractional behav-

ior. Such models provide deeper insights into the memory effects and anomalous diffusion in biological systems [1, 22, 3]. The extended Euler method for fractional-order systems provides a numerical approach for approximating the solutions of differential equations that involve memory effects. This is particularly effective for systems modeled using Caputo fractional derivatives that incorporate the initial conditions in a physically meaningful manner. This method discretizes the fractional derivative by considering the entire history of the solution and capturing long-term dynamics more accurately. It is widely used because of its simplicity, efficiency, and suitability for simulating complex real-world processes governed by noninteger order dynamics [12, 11, 6, 26].

The primary objective of this study is to analyze and solve a double-intermediate enzyme reaction model using the fractional Caputo derivative within the framework of the generalized Euler method. Fractional calculus is appropriate because enzymatic reactions exhibit hereditary properties and distributed time delays owing to multiple intermediate complexes and conformational changes. The fractional order (ς) quantifies this memory effect by bridging the instantaneous kinetics (integer order) and long-term hereditary responses (noninteger order). This improves the realism of the biochemical model. The remainder of this paper is organized as follows: Section 2 outlines the basic definitions and properties of the fractional calculus. In section 3, the proposed model is formulated in dimensionless form and subsequently transformed into its fractional Caputo derivative. Section 4 presents a theoretical analysis of key theorems related to the proposed model. Section 5 details the numerical solution of the model using the generalized Euler method and discusses the obtained results. Finally, section 6 summarizes the findings and outlines the possible directions for future research.

2 Preliminaries

This section introduces the essential mathematical background and foundational concepts of fractional calculus that are crucial for the mathematical formulation of the proposed model.

Definition 1 (Fractional integral in the Riemann–Liouville sense [7])**.** Let $f : \mathbb{R}_+ \to \mathbb{R}$ be a real-valued function, and let $\varsigma > 0$. The Riemann–Liouville fractional integral of order ς is defined as

$$\mathcal{I}_t^{\varsigma} f(t) = \frac{1}{\Gamma(\varsigma)} \int_0^t (t-\tau)^{\varsigma-1} f(\tau)\, d\tau, \tag{1}$$

where $\Gamma(\cdot)$ denotes the Gamma function.

Definition 2 (Caputo fractional derivative [6])**.** For $0 < \varsigma \leq 1$ and $f \in C^1([0,\infty))$, the Caputo derivative of the order ς is given by

$$ {}^{C}D_t^{\varsigma} f(t) = \frac{1}{\Gamma(1-\varsigma)} \int_0^t f'(s)(t-s)^{-\varsigma}\, ds. \tag{2} $$

Definition 3 (Mittag–Leffler functions [15])**.** The generalized Mittag–Leffler functions with one and two parameters are defined by the following power series expansions:

$$ \mathbb{E}_{\alpha}(z) = \sum_{k=0}^{\infty} \frac{z^k}{\Gamma(\alpha k + 1)}, \quad \alpha > 0, \tag{3} $$

$$ \mathbb{E}_{\alpha,\beta}(z) = \sum_{k=0}^{\infty} \frac{z^k}{\Gamma(\alpha k + \beta)}, \quad \alpha > 0, \beta > 0. \tag{4} $$

These functions serve as natural generalizations of the exponential function and are widely used in fractional calculus.

Definition 4 (Euler's Gamma function [12, 26])**.** For any real number $x > 0$, the Gamma function is defined by the integral

$$ \Gamma(x) = \int_0^{\infty} t^{x-1} e^{-t}\, dt. \tag{5} $$

Lemma 1. Let $f \in L^{\infty}(\mathbb{R}) \cap \mathcal{B}(\mathbb{R})$ and let $\varsigma \in \mathbb{R}$ with $n-1 < \varsigma < n$, where $n \in \mathbb{N}$. Then, the following properties hold:

1. $\mathcal{D}_t^{\varsigma}\, \mathcal{I}_t^{\varsigma} f(t) = f(t)$,
2. $\mathcal{I}_t^{\varsigma}\, \mathcal{D}_t^{\varsigma} f(t) = f(t) - \sum_{k=0}^{n-1} \frac{t^k}{k!} f^{(k)}(0)$.

3 Formulation of the model

The dynamics of enzyme-catalyzed reactions with two intermediate complexes have been previously analyzed using classical integer-order differential equation models [5, 23]. These models capture the stepwise kinetics of enzyme-substrate interactions, emphasizing the transient behavior and steady-state approximations of the intermediate species. Building on this foundation, we extend the analysis by incorporating fractional-order derivatives to account for memory effects and anomalous kinetics inherent in biochemical systems.

Consider a model of a double intermediate enzyme-catalyst reaction:

$$ \mathcal{E}_n + \mathcal{S}_u \underset{\kappa_{-1}}{\overset{\kappa_1}{\longleftrightarrow}} \mathcal{Y} \xrightarrow{\kappa_2} \mathcal{Z} \xrightarrow{\kappa_3} \mathcal{E}_n + \mathcal{P}_r. \tag{6} $$

An enzyme ($\mathcal{E}_n$) interacts reversibly with a substrate ($\mathcal{S}_u$) to form an intermediate complex ($\mathcal{Y}$) known as the enzyme-substrate complex. This intermediate is then irreversibly transformed into another enzyme-substrate complex ($\mathcal{Z}$), which subsequently dissociates to release the original enzyme ($\mathcal{E}_n$) and the final product ($\mathcal{P}_r$). The process involves rate constants κ_1, κ_{-1}, κ_2, and κ_3. Based on the assumption that the reverse reactions involving κ_{-2} and κ_{-3} are negligible owing to their low rates, these steps are effectively treated as irreversible reactions. Figure 1 illustrates the transmission of the double intermediate enzyme reaction model.

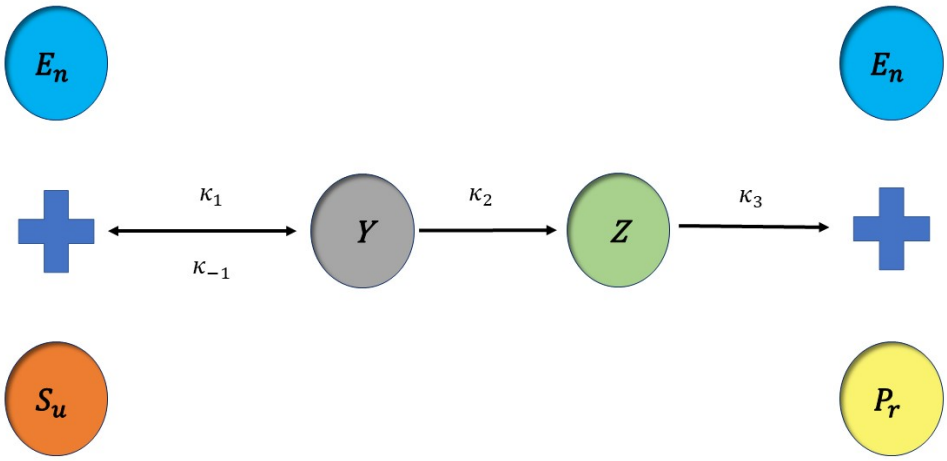

Figure 1: Flowchart of the double intermediate enzyme reaction model

The reaction kinetics, following the law of mass action, are governed by

$$\frac{d\mathcal{S}_u}{d\tau} = -\kappa_1 \mathcal{S}_u \mathcal{E}_n + \kappa_{-1} \mathcal{Y}, \tag{7}$$

$$\frac{d\mathcal{E}_n}{d\tau} = -\kappa_1 \mathcal{S}_u \mathcal{E}_n + \kappa_{-1} \mathcal{Y} + \kappa_3 \mathcal{Z}, \tag{8}$$

$$\frac{d\mathcal{Y}}{d\tau} = \kappa_1 \mathcal{S}_u \mathcal{E}_n - (\kappa_{-1} + \kappa_2) \mathcal{Y}, \tag{9}$$

$$\frac{d\mathcal{Z}}{d\tau} = \kappa_2 \mathcal{Y} - \kappa_3 \mathcal{Z}, \tag{10}$$

$$\frac{d\mathcal{P}_r}{d\tau} = \kappa_3 \mathcal{Z}, \tag{11}$$

with the following initial conditions:

$$\mathcal{E}_n(0) = \mathcal{E}_{n0}, \quad \mathcal{S}_u(0) = \mathcal{S}_{u0}, \quad \mathcal{Y}(0) = 0, \quad \mathcal{Z}(0) = 0, \quad \mathcal{P}_r(0) = 0. \tag{12}$$

By applying the conservation relationships corresponding to (7)–(11), together with the initial conditions specified in (12), the following equations are obtained:

$$\mathcal{E}_n + \mathcal{Y} + \mathcal{Z} = \mathcal{E}_{n0}, \quad \mathcal{S}_u + \mathcal{Y} + \mathcal{Z} + \mathcal{P}_r = \mathcal{S}_{u0}. \tag{13}$$

Adding (10) and (11) yields

$$\frac{d\mathcal{Z}}{d\tau} + \frac{d\mathcal{P}_r}{d\tau} = \kappa_2 \mathcal{Y}. \tag{14}$$

After the pre-steady-state phase, the reaction rate involving the formation of complex $\mathcal{P}_r + 2$ reaches a stable level, leading to an approximately constant concentration of the initial enzyme-substrate complex, $\mathcal{Y}$. At this stage, the derivative of $\mathcal{Y}$ becomes negligible and can be approximated as zero. By combining this condition with the conservation relation given in (13), $\mathcal{Y}$ can be expressed as a function of $\mathcal{S}$ and $\mathcal{Z}$ as follows:

$$\mathcal{Y} = \frac{(\mathcal{E}_{n0} - \mathcal{Z})\mathcal{S}_u}{\mathcal{K} + \mathcal{S}_u}, \tag{15}$$

where the Michaelis constant $\mathcal{K}$ is defined as

$$\mathcal{K} = \frac{\kappa_{-1} + \kappa_2}{\kappa_1}. \tag{16}$$

According to (15), the variable reaches a steady state, based on the current values of $\mathcal{S}_u$ and $\mathcal{Z}$. Although (7) and (10) govern the dynamics of $\mathcal{S}_u$ and $\mathcal{Z}$, it is challenging to uphold earlier heuristic reasoning because of uncertainties regarding the relative magnitudes of the variables involved. In certain cases, $\mathcal{Z}$ can be considered negligible if it is significantly smaller than (15). Substituting (15) into (7) yields

$$\frac{d\mathcal{S}_u}{d\tau} = -\frac{\kappa_2 \mathcal{E}_{n0} \mathcal{S}_u}{\mathcal{K} + \mathcal{S}_u}. \tag{17}$$

By using the initial condition $\mathcal{S}_u(0) = \mathcal{S}_{u0}$ and (17), we can approximate the behavior of $\mathcal{S}$ under the assumption that the substrate concentration changes only slightly during the steady-state phase. However, the role of $\mathcal{Z}$ in comparison to $\mathcal{E}_{n0}$ remains to be evaluated. Notably, $\mathcal{Z}$ is expected to increase rapidly from zero during the pre-steady state because the sum $\mathcal{P}_r + \mathcal{Z}$ (related to (10) and (11)) is proportional to $\mathcal{Y}$.

A crucial step in simplifying the problem is reformulating it as a reduced system of differential equations. This approach involves removing $\mathcal{E}_n$ using the conservation relation $\mathcal{E}_n = \mathcal{E}_{n0} - \mathcal{Y} - \mathcal{Z}$ from (13), and determining $\mathcal{P}_r$ in terms of $\mathcal{Z}$, as described in (10). Consequently, the following equations are obtained

$$\frac{d\mathcal{S}_u}{d\tau} = -\kappa_1 \mathcal{S}_u(\mathcal{E}_{n0} - \mathcal{Y} - \mathcal{Z}) + \kappa_{-1}\mathcal{Y}, \tag{18}$$

$$\frac{d\mathcal{Y}}{d\tau} = \kappa_1 \mathcal{S}_u(\mathcal{E}_{n0} - \mathcal{Y} - \mathcal{Z}) - (\kappa_{-1} + \kappa_2)\mathcal{Y}, \tag{19}$$

$$\frac{d\mathcal{Z}}{d\tau} = \kappa_2 \mathcal{Y} - \kappa_3 \mathcal{Z}, \tag{20}$$

with the following initial conditions:

$$\mathcal{S}_u(0) = \mathcal{S}_{u0}, \quad \mathcal{Y}(0) = 0, \quad \mathcal{Z}(0) = 0. \tag{21}$$

To advance the analysis in a structured manner, it is necessary to nondimensionalize the system at this stage. This involves defining the following dimensionless variables and parameters:

$$\begin{gathered} \mathcal{S}_u = \delta \mathcal{U}, \quad \mathcal{Y} = \varpi \mathcal{V}, \quad \mathcal{Z} = \gamma \mathcal{W}, \quad \tau = \mathcal{V}t, \quad \gamma = \mathcal{E}_{n0}, \quad \delta = \mathcal{S}_{u0}, \\ \varpi = \frac{\mathcal{E}_{n0}\mathcal{S}_{u0}}{\mathcal{S}_{u0} + \mathcal{K}}, \quad \vartheta = \frac{\mathcal{S}_{u0}}{\mathcal{K}}, \quad \sigma = \frac{\kappa_{-1}}{\kappa_2}, \quad \phi = \frac{\kappa_3(\kappa_{-1} + \kappa_2)}{\kappa_1}. \end{gathered} \tag{22}$$

Accordingly, using (22), the system (18)–(20) is transformed into the following dimensionless form:

$$\frac{d\mathcal{U}}{dt} = -\varpi \mathcal{U} + \vartheta\theta\varpi \mathcal{U}\mathcal{V} + \varpi \mathcal{U}\mathcal{W} + \theta\alpha\varpi\sigma\mathcal{V}, \tag{23}$$

$$\frac{d\mathcal{V}}{dt} = \mathcal{U} - \vartheta\theta\mathcal{U}\mathcal{V} - \mathcal{U}\mathcal{W} - \theta\mathcal{V}, \tag{24}$$

$$\frac{d\mathcal{W}}{dt} = \vartheta\theta^2\alpha\mathcal{V} - \phi\theta\mathcal{W}. \tag{25}$$

To simplify the analysis, the following dimensionless parameter values were assumed:

$$\theta = \frac{1}{1+\vartheta}, \quad \alpha = \frac{1}{1+\sigma},$$

with the following dimensionless initial conditions from (21):

$$\mathcal{U}(0) = 1, \quad \mathcal{V}(0) = 0, \quad \mathcal{W}(0) = 0. \tag{26}$$

The proposed double-enzyme reaction system (23)–(25) is formulated in fractional order using the Caputo fractional derivative [6, 25] as follows:

$${}^{C}D_t^{\varsigma}\mathcal{U} = -\varpi \mathcal{U} + \vartheta\theta\varpi \mathcal{U}\mathcal{V} + \varpi \mathcal{U}\mathcal{W} + \theta\alpha\varpi\sigma\mathcal{V}, \tag{27}$$

$${}^{C}D_t^{\varsigma}\mathcal{V} = \mathcal{U} - \vartheta\theta\mathcal{U}\mathcal{V} - \mathcal{U}\mathcal{W} - \theta\mathcal{V}, \tag{28}$$

$${}^{C}D_t^{\varsigma}\mathcal{W} = \vartheta\theta^2\alpha\mathcal{V} - \phi\theta\mathcal{W}, \tag{29}$$

with the following initial conditions:

$$\mathcal{U}(0) = 1, \quad \mathcal{V}(0) = 0, \quad \mathcal{W}(0) = 0, \tag{30}$$

where ${}^{C}D_t^{\varsigma}$ denotes the Caputo fractional derivative of order ς, and ς represents the fractional time derivative.

4 Analysis of the model

In this section, we aim to establish the positivity, boundedness, existence, and uniqueness of the solutions, which are essential properties for validating the mathematical consistency of the proposed double-enzyme reaction fraction model.

4.1 Positivity and boundedness

Theorem 1. For the dimensionless concentrations ($\mathcal{U} \geq 0$, $\mathcal{V} \geq 0$, $\mathcal{W} \geq 0$) and nonnegative dimensionless parameters associated with the variables, the solution of the system in (27)–(29) is nonnegative for all $t > 0$.

Proof. From (27), we have

$$\frac{d\mathcal{U}}{dt} + \varpi\mathcal{U} - \vartheta\theta\varpi\mathcal{U}\mathcal{V} - \varpi\mathcal{U}\mathcal{W} - \theta\alpha\varpi\sigma\mathcal{V} = 0 \tag{31}$$

implies

$$\frac{d\mathcal{U}}{dt} = -(\varpi\mathcal{U} - \vartheta\theta\varpi\mathcal{U}\mathcal{V} - \varpi\mathcal{U}\mathcal{W} - \theta\alpha\varpi\sigma\mathcal{V}). \tag{32}$$

Then,

$$\frac{d\mathcal{U}}{dt} \geq -(\varpi\mathcal{U} - \vartheta\theta\varpi\mathcal{U}\mathcal{V} - \varpi\mathcal{U}\mathcal{W}), \tag{33}$$

$$\frac{d\mathcal{U}}{\mathcal{U}} \geq -(\varpi - \vartheta\theta\varpi\mathcal{V} - \varpi\mathcal{W})dt. \tag{34}$$

Now, we have

$$\ln(\mathcal{U}(t)) \geq -\int(\varpi - \vartheta\theta\varpi\mathcal{V} - \varpi\mathcal{W})dt + C. \tag{35}$$

Define

$$\mathcal{L}(t) = -\int(\varpi - \vartheta\theta\varpi\mathcal{V} - \varpi\mathcal{W})dt, \tag{36}$$

which follows that

$$\ln(\mathcal{U}(t)) \geq \mathcal{L}(t) + C. \tag{37}$$

At $t = 0$, we have

$$\ln(\mathcal{U}(0)) \geq \mathcal{L}(0) + C. \tag{38}$$

From (37) and (38), we obtain

$$\ln\left(\frac{\mathcal{U}(t)}{\mathcal{U}(0)}\right) \geq \mathcal{L}(t) - \mathcal{L}(0). \tag{39}$$

By multiplying both sides exponentially, we obtain

$$\mathcal{U}(t) \geq \mathcal{U}(0)e^{\mathcal{L}(t)-\mathcal{L}(0)} \geq \mathcal{U}(0). \tag{40}$$

Since $\mathcal{U}(0) = \mathcal{U}_0$ is positive,

$$\mathcal{U}(t) \geq \mathcal{U}(0) > 0 \quad \text{for all} \quad t > 0. \tag{41}$$

Hence, it follows that $\mathcal{U}(t) \geq 0$ for all $t > 0$, confirming that the dimensionless concentration $\mathcal{U}(t)$ remains nonnegative over time. The same procedure applies to other dimensionless state variables, demonstrating that $\mathcal{V}(t)$ and $\mathcal{W}(t)$ are nonnegative for $t > 0$. □

Theorem 2. The solution of the dimensionless system (27)–(29) lies entirely in the invariant region $\Omega = \{(\mathcal{U}, \mathcal{V}, \mathcal{W}) \in \mathbb{R}^3_+ \mid \mathcal{U} + \mathcal{V} + \mathcal{W} = \mathcal{N}\}$, which is bounded.

Proof. The total dimensionless concentration $\mathcal{N}$ can be determined by combining (27)–(29), which can be written as

$$\mathcal{N}(t) = \mathcal{U}(t) + \mathcal{V}(t) + \mathcal{W}(t). \tag{42}$$

Differentiating with respect to t, we obtain

$$\frac{d\mathcal{N}}{dt} = \frac{d\mathcal{U}}{dt} + \frac{d\mathcal{V}}{dt} + \frac{d\mathcal{W}}{dt}. \tag{43}$$

Then,

$$\begin{aligned} \frac{d\mathcal{N}}{dt} =& (-\varpi\mathcal{U} + \vartheta\theta\varpi\mathcal{U}\mathcal{V} + \varpi\mathcal{U}\mathcal{W} + \theta\alpha\varpi\sigma\mathcal{V}) \\ &+ (\mathcal{U} - \vartheta\theta\mathcal{U}\mathcal{V} - \mathcal{U}\mathcal{W} - \theta\mathcal{V}) + (\vartheta\theta^2\alpha\mathcal{V} - \phi\theta\mathcal{W}). \end{aligned} \tag{44}$$

After simplification,

$$\frac{d\mathcal{N}}{dt} = (1-\varpi)\mathcal{U} + (\theta\alpha\varpi\sigma)\mathcal{V} - \phi\theta\mathcal{W} + (\vartheta\theta\varpi - \vartheta\theta)\mathcal{U}\mathcal{V} + (\varpi - 1)\mathcal{U}\mathcal{W}. \tag{45}$$

If all dimensionless parameters are nonnegative, the terms involving $\mathcal{U}, \mathcal{V}, \mathcal{W}$ are bounded. Thus, $\frac{d\mathcal{N}}{dt}$ is bounded and $\mathcal{N}(t)$ does not increase indefinitely. Since $N = \mathcal{U} + \mathcal{V} + \mathcal{W}$ remains bounded and nonnegative for $\mathcal{U}$, $\mathcal{V}$, and $\mathcal{W}$, the system evolves within the region

$$\Omega = \{(\mathcal{U}, \mathcal{V}, \mathcal{W}) \in \mathbb{R}^3_+ \mid \mathcal{U} + \mathcal{V} + \mathcal{W} \leq N_0\}, \tag{46}$$

where $\mathcal{N}_0 = \mathcal{U}(0) + \mathcal{V}(0) + \mathcal{W}(0)$ denotes the total initial value.

Thus, region Ω is positively invariant, meaning that solutions starting in Ω remain in Ω for all $t \geq 0$. (ii) This ensures that the system is feasible and functions appropriately. □

4.2 Uniqueness and existence

Theorem 3. A unique solution exists within the feasible region of the dimensionless fractional-order system (27)–(29), provided that the initial conditions are nonnegative.

Proof. To establish the existence and uniqueness of the dimensionless fractional-order model, we adopt the method outlined in [14], considering the feasible region as $\Psi \times (0, T]$, where Ψ is defined as

$$\Psi = \{(\mathcal{U}, \mathcal{V}, \mathcal{W}) \in \mathbb{R}^3_+ : \max(|\mathcal{U}|, |\mathcal{V}|, |\mathcal{W}|) \leq \rho\}. \tag{47}$$

Consider the mapping

$$\Theta = (\Theta_1(\xi), \Theta_2(\xi), \Theta_3(\xi)), \tag{48}$$

and

$$\begin{aligned} \Theta_1(\xi) &= -\varpi\mathcal{U} + \vartheta\theta\varpi\mathcal{U}\mathcal{V} + \varpi\mathcal{U}\mathcal{W} + \theta\alpha\varpi\sigma\mathcal{V}, \\ \Theta_2(\xi) &= \mathcal{U} - \vartheta\theta\mathcal{U}\mathcal{V} - \mathcal{U}\mathcal{W} - \theta\mathcal{V}, \\ \Theta_3(\xi) &= \vartheta\theta^2\alpha\mathcal{V} - \phi\theta\mathcal{W}. \end{aligned} \tag{49}$$

We denote $\xi = (\mathcal{U}, \mathcal{V}, \mathcal{W})$ and $\bar{\xi} = (\bar{\mathcal{U}}, \bar{\mathcal{V}}, \bar{\mathcal{W}})$. For any $\xi, \bar{xi} \in \Psi$, from (49), we obtain that

$$\|\Theta(\xi) - \Theta(\bar{\xi})\| = |\Theta_1(\xi) - \Theta_1(\bar{\xi})| + |\Theta_2(\xi) - \Theta_2(\bar{\xi})| + |\Theta_3(\xi) - \Theta_3(\bar{\xi})|. \tag{50}$$

Using the values of $\Theta_i(\xi)$ and $\Theta_i(\bar{\xi})$, $i = 1, 2, 3$, we obtain

$$\begin{aligned}
&\|\Theta(\xi)-\Theta(\bar{\xi})\| \\
&=|-\varpi\mathcal{U}+\vartheta\theta\varpi\mathcal{U}\mathcal{V}+\varpi\mathcal{U}\mathcal{W}+\theta\alpha\varpi\sigma\mathcal{V}+\varpi\bar{\mathcal{U}}-\vartheta\theta\varpi\bar{\mathcal{U}}\bar{\mathcal{V}}-\varpi\bar{\mathcal{U}}\bar{\mathcal{W}}-\theta\alpha\varpi\sigma\bar{\mathcal{V}}| \\
&\quad+|\mathcal{U}-\vartheta\theta\mathcal{U}\mathcal{V}-\mathcal{U}\mathcal{W}-\theta\mathcal{V}-\bar{\mathcal{U}}+\vartheta\theta\bar{\mathcal{U}}\bar{\mathcal{V}}+\bar{\mathcal{U}}\bar{\mathcal{W}}+\theta\bar{\mathcal{V}}| \\
&\quad+|\vartheta\theta^2\alpha\mathcal{V}-\phi\theta\mathcal{W}-\vartheta\theta^2\alpha\bar{\mathcal{V}}+\phi\theta\bar{\mathcal{W}}|.
\end{aligned} \tag{51}$$

Rearranging the terms, we have

$$\begin{aligned}
&\|\Theta(\xi)-\Theta(\bar{\xi})\| \\
&=|-\varpi\mathcal{U}+\varpi\bar{\mathcal{U}}+\vartheta\theta\varpi\mathcal{U}\mathcal{V}-\vartheta\theta\varpi\bar{\mathcal{U}}\bar{\mathcal{V}}+\varpi\mathcal{U}\mathcal{W}-\varpi\bar{\mathcal{U}}\bar{\mathcal{W}}+\theta\alpha\varpi\sigma\mathcal{V}-\theta\alpha\varpi\sigma\bar{\mathcal{V}}| \\
&\quad+|\mathcal{U}-\bar{\mathcal{U}}-\vartheta\theta\mathcal{U}\mathcal{V}+\vartheta\theta\bar{\mathcal{U}}\bar{\mathcal{V}}-\mathcal{U}\mathcal{W}+\bar{\mathcal{U}}\bar{\mathcal{W}}-\theta\mathcal{V}+\theta\bar{\mathcal{V}}| \\
&\quad+|\vartheta\theta^2\alpha\mathcal{V}-\vartheta\theta^2\alpha\bar{\mathcal{V}}-\phi\theta\mathcal{W}+\phi\theta\bar{\mathcal{W}}|.
\end{aligned} \tag{52}$$

Using the mean value theorem, we have

$$\begin{aligned}
&\|\Theta(\xi)-\Theta(\bar{\xi})\| \\
&\leq\varpi|\mathcal{U}-\bar{\mathcal{U}}|+\vartheta\theta\varpi\rho[|\mathcal{U}-\bar{\mathcal{U}}|+|\mathcal{V}-\bar{\mathcal{V}}|]+\varpi\rho[|\mathcal{U}-\bar{\mathcal{U}}|+|\mathcal{W}-\bar{\mathcal{W}}|] \\
&\quad+\theta\alpha\varpi\sigma|\mathcal{V}-\bar{\mathcal{V}}|+|\mathcal{U}-\bar{\mathcal{U}}|+\vartheta\theta\rho[|\mathcal{U}-\bar{\mathcal{U}}|+|\mathcal{V}-\bar{\mathcal{V}}|]+\rho[|\mathcal{U}-\bar{\mathcal{U}}|+|\mathcal{W}-\bar{\mathcal{W}}|] \\
&\quad+\theta|\mathcal{V}-\bar{\mathcal{V}}|+\vartheta\theta^2\alpha|\mathcal{V}-\bar{\mathcal{V}}|+\phi\theta|\mathcal{W}-\bar{\mathcal{W}}|.
\end{aligned} \tag{53}$$

After simplification, we obtain

$$\begin{aligned}
&\|\Theta(\xi)-\Theta(\bar{\xi})\| \\
&\leq(\varpi+\vartheta\theta\varpi\rho+\varpi\rho+1+\vartheta\theta\rho+\rho)|\mathcal{U}-\bar{\mathcal{U}}| \\
&\quad+(\vartheta\theta\varpi\rho+\theta\alpha\varpi\sigma+\vartheta\theta\rho+\theta+\vartheta\theta^2\alpha)|\mathcal{V}-\bar{\mathcal{V}}|+(\varpi\rho+\rho+\phi\theta)|\mathcal{W}-\bar{\mathcal{W}}|.
\end{aligned} \tag{54}$$

Thus,

$$\|\Theta(\xi)-\Theta(\bar{\xi})\|\leq\Omega||\xi-\bar{\xi}||, \tag{55}$$

where $Q_1=(\varpi+\vartheta\theta\varpi\rho+\varpi\rho+1+\vartheta\theta\rho+\rho)$, $Q_2=(\vartheta\theta\varpi\rho+\theta\alpha\varpi\sigma+\vartheta\theta\rho+\theta+\vartheta\theta^2\alpha)$, $Q_3=(\varpi\rho+\rho+\phi\theta)$, and $\Omega=\max\{Q_1,Q_2,Q_3\}$.

Therefore, $\Theta(\xi)$ satisfies the Lipschitz condition with respect to ξ. Consequently, the existence and uniqueness of the solution to the dimensionless fractional-order model were guaranteed. □

Theorem 4. The dimensionless model (27)–(29) comprises a unique solution $\xi(t)\in\Psi$ for the given dimensionless initial condition ξ_0 for each $\xi_0=\{\mathcal{U}_0,\mathcal{V}_0,\mathcal{W}_0\}$ for all $t\geq 0$.

5 Numerical simulation

5.1 Extended Euler approach

Motivated by fractional numerical techniques, we adopted the extend Euler method to approximate the solutions for a given system. First, we consider fractional-order differential equations [12, 11, 6, 26]:

$$\mathcal{F}^{\varsigma} w = f(t, w), \quad t \in [0, T], \quad 0 < \varsigma \leq 1. \tag{56}$$

To numerically approximate the solution of the fractional-order differential equation, we divided the interval $[0, c]$ into k subintervals of uniform length $h = \frac{c}{k}$. The corresponding time points are denoted as $t_i = jh$ for $i = 0, 1, \ldots, k$. Assuming that the function $w(t)$ and its fractional derivatives $\mathcal{F}^{\varsigma} w(t)$ and $\mathcal{F}^{2\varsigma} w(t)$ are continuous in the interval $[0, c]$, we can utilize a fractional Taylor series expansion to approximate the solution, as follows:

$$w(t) = w(t_0) + \left(\mathcal{F}^{\varsigma} w(t_0)\right) \frac{t^{\varsigma}}{\Gamma(\varsigma + 1)} + \left(\mathcal{F}^{2\varsigma} w(a_1)\right) \frac{t^{2\varsigma}}{\Gamma(2\varsigma + 1)}. \tag{57}$$

By replacing the fractional derivative $\mathcal{F}^{\varsigma} w(t_0)$ with the function $f(t_0, w(t_0))$ and omitting the higher-order term for a small step size h, the approximation at the next time step becomes

$$w(t_1) = w(t_0) + \frac{h^{\varsigma}}{\Gamma(\varsigma + 1)} f(t_0, w(t_0)). \tag{58}$$

This approach can be applied iteratively to obtain solutions at subsequent time points. Thus, for a general step $t_{i+1} = t_i + h$, the extended Euler approximation for the fractional-order case is

$$w(t_{j+1}) = w(t_j) + \frac{h^{\varsigma}}{\Gamma(\varsigma + 1)} f(t_j, w(t_j)), \quad j = 0, 1, \ldots, k - 1. \tag{59}$$

When the fractional order $\varsigma = 1$, this formulation is naturally reduced to the classical Euler method used for ordinary differential equations.

Applying this extended numerical approach (59) to the given dimensionless system (27)–(29) yields the following iterative expressions:

$$\mathcal{U}_h^{(n+1)} = \mathcal{U}_h^n + \frac{h^{\varsigma}}{\Gamma(\varsigma + 1)} [-\varpi \mathcal{U} + \vartheta \theta \varpi \mathcal{U} \mathcal{V} + \varpi \mathcal{U} \mathcal{W} + \theta \alpha \varpi \sigma \mathcal{V}], \tag{60}$$

$$\mathcal{V}_h^{(n+1)} = \mathcal{V}_h^n + \frac{h^{\varsigma}}{\Gamma(\varsigma + 1)} [\mathcal{U} - \vartheta \theta \mathcal{U} \mathcal{V} - \mathcal{U} \mathcal{W} - \theta \mathcal{V}], \tag{61}$$

$$\mathcal{W}_h^{(n+1)} = \mathcal{W}_h^n + \frac{h^{\varsigma}}{\Gamma(\varsigma + 1)} [\vartheta \theta^2 \alpha \mathcal{V} - \phi \theta \mathcal{W}]. \tag{62}$$

This can be rewritten as

$$\mathcal{U}_h^{(n+1)} = \mathcal{U}_h^n + \beth[-\varpi\mathcal{U} + \vartheta\theta\varpi\mathcal{U}\mathcal{V} + \varpi\mathcal{U}\mathcal{W} + \theta\alpha\varpi\sigma\mathcal{V}], \tag{63}$$

$$\mathcal{V}_h^{(n+1)} = \mathcal{V}_h^n + \beth[\mathcal{U} - \vartheta\theta\mathcal{U}\mathcal{V} - \mathcal{U}\mathcal{W} - \theta\mathcal{V}], \tag{64}$$

$$\mathcal{W}_h^{(n+1)} = \mathcal{W}_h^n + \beth[\vartheta\theta^2\alpha\mathcal{V} - \phi\theta\mathcal{W}], \tag{65}$$

where the parameter $0 < \beth = \frac{h^\varsigma}{\Gamma(\varsigma+1)} < 1$ serves as the step size and the initial values at fixed points are $\mathcal{U}(0) = \mathcal{U}_0$, $\mathcal{V}(0) = \mathcal{V}_0$, and $\mathcal{W}(0) = \mathcal{W}_0$. This extended numerical scheme is an effective tool for approximating fractional dynamics while maintaining the computational efficiency.

5.2 Numerical experiments and discussions

This subsection presents the dynamic behavior of the proposed fractional-order model based on dimensionless concentrations and parameters. Numerical simulations were performed using MATLAB® to analyze the system response. In the context of this enzymatic reaction model, the dimensionless parameters ϖ, ϑ, σ, and ϕ play significant roles in shaping the biochemical behavior of the system. From a chemical perspective, ϖ quantifies the effective catalytic potential of the enzyme-substrate interaction, reflecting the extent to which the enzyme is engaged in catalysis under given initial conditions. Parameter ϑ represents the ratio of the initial substrate concentration to the Michaelis constant, thus capturing the level of substrate saturation; higher values indicate near-saturation and maximal enzyme activity. The parameter σ characterizes the reversibility of the first enzyme-substrate complex, with larger values suggesting a greater tendency for the complex to dissociate back to the reactants rather than proceed to the next step. Finally, ϕ incorporates the effects of multiple rate constants and represents the overall catalytic throughput, indicating the efficiency of the system in progressing toward product formation.

Figure 2 illustrates the behavior of the dimensionless concentrations $\mathcal{U}$, $\mathcal{V}$, and $\mathcal{W}$ under fixed dimensionless parameter values ($\varpi = \vartheta = \sigma = \phi = 0.01$) over a dimensionless distance of 1 as the fractional order ς varies from 0.6 to 1. In Figure 2a, increasing the fractional order ς led to an increase in the concentration of $\mathcal{U}$. In Figure 2b, as the fractional order ς increased, the concentration of $\mathcal{V}$ decreased. Similarly, Figure 2c shows that increasing the fractional order ς decreased the concentration of $\mathcal{W}$. Notably, all concentrations behave uniformly for $\mathcal{U}, \mathcal{V}, \mathcal{W} \approx 1$.

Figure 3 presents the dynamics of the concentrations $\mathcal{U}$, $\mathcal{V}$, and $\mathcal{W}$ for different dimensionless parameters ($\varpi = 2$, $\vartheta = 0.01$, $\sigma = 0.01$, $\phi = 0.5$) over a dimensionless distance of 10, as the fractional order ς varies from 0.6 to 1. In Figure 3a, an increase in ς causes the concentration

of $\mathcal{U}$ to decrease for $t < 2$ and all solutions tend toward zero thereafter. In Figure 3b, the concentration $\mathcal{V}$ decreases after specific time intervals and approaches zero in all cases after $t < 6$ s. In Figure 3c, as ς increased, the concentration $\mathcal{W}$ decreased at various time intervals. Figure 4 shows the effect of varying dimensionless parameter ϖ on dimensionless concentrations $\mathcal{U}$, $\mathcal{V}$, and $\mathcal{W}$ with fixed values of $\vartheta = 0.01$, $\sigma = 0.01$, and $\phi = 0.5$. Here, the fractional order is fixed at $\varsigma = 1$, which corresponds to classical derivatives. In Figures 4a–4c, an increase in ϖ results in a decrease in all three concentrations, $\mathcal{U}$, $\mathcal{V}$, and $\mathcal{W}$.

Figure 5 shows the impact of the dimensionless parameter ϑ on $\mathcal{U}$, $\mathcal{V}$, and $\mathcal{W}$, while keeping $\varpi = 2$, $\sigma = 0.5$, and $\phi = 0.05$ constant and using the classical case $\varsigma = 1$. In Figures 5a–5c, increasing ϑ leads to an increase in the concentrations $\mathcal{U}$, $\mathcal{V}$, and $\mathcal{W}$. Figure 6 shows the effect of varying the dimensionless parameter σ on $\mathcal{U}$, $\mathcal{V}$, and $\mathcal{W}$ with fixed values of $\varpi = 2$, $\vartheta = 0.01$, $\phi = 0.05$, and fractional order $\varsigma = 1$. In Figures 6a and 6b, as σ increases, the concentrations $\mathcal{U}$ and $\mathcal{V}$ increase. However, in Figure 6c, the concentration $\mathcal{W}$ decreases as σ increases, which is contrary.

Figure 7 shows the behavior of $\mathcal{U}$, $\mathcal{V}$, and $\mathcal{W}$ as the dimensionless parameter ϕ varies, with $\varpi = 2$, $\vartheta = 0.01$, and $\sigma = 0.01$ fixed, and the fractional order $\varsigma = 1$. In Figures 7a and 7b, changes in ϕ do not affect the concentrations $\mathcal{U}$ and $\mathcal{V}$, which remain constant. In Figure 7c, however, the concentration $\mathcal{W}$ decreases as ϕ increases, which is a contradiction.

Figure 8 shows the surface plots and heat maps of the dimensionless concentration $\mathcal{U}$ for different values of dimensionless parameters ϖ, ϑ, σ, and ϕ. In Figure 8a, the combined influence of ϖ and σ on the concentration $\mathcal{U}$ is presented, which captures their interactive effects on system behavior. Figure 8b shows the combined impact of ϑ and ϕ on $\mathcal{U}$, further revealing how these dimensionless parameters influence concentration through their variations. Dark pink indicates regions of high parameter impact, light blue indicates regions of low impact, and intermediate colors reflect varying degrees of transmission intensity for the selected parameters. Similarly, the same scenarios were analyzed for concentrations $\mathcal{V}$ and $\mathcal{W}$ in Figures 9 and 10, respectively. These visualizations offer valuable insights into the parameter sensitivity and multidimensional dependence of concentrations $\mathcal{U}$, $\mathcal{V}$ and $\mathcal{W}$.

Figure 11 presents pie charts illustrating the distribution of the dimensionless parameters for the two cases. The parameter values on the left side are $\varpi = 2$, $\vartheta = 0.1$, $\sigma = 0.1$, and $\phi = 0.5$. This configuration represents a scenario in which ϖ is dominant, and the remaining parameters have relatively low magnitudes. On the right-hand side, the pie chart shows the distribution for an alternative case with $\varpi = 10$, $\vartheta = 5$, $\sigma = 1$, and $\phi = 2$. Compared with the previous case, all the parameters exhibited larger values, and their proportional contributions varied significantly. These visualizations provide a clear comparison of the relative contributions of the dimensionless parameters under varying conditions.

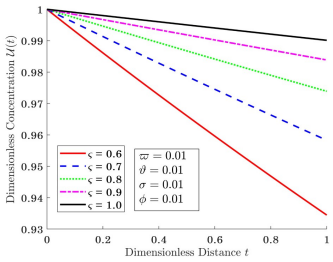

(a) Dimensionless concentration $\mathcal{U}(t)$

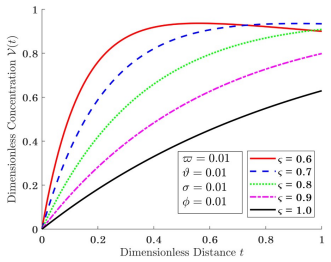

(b) Dimensionless concentration $\mathcal{V}(t)$

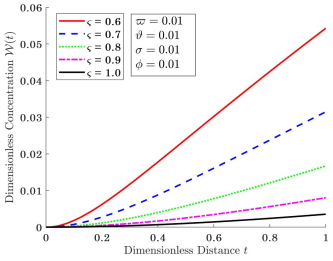

(c) Dimensionless concentration $\mathcal{W}(t)$

Figure 2: Graphical representation of the dimensionless concentrations $\mathcal{U}, \mathcal{V}, \mathcal{W}$ for fixed dimensionless parameters under varying fractional orders ς $(0.6 - 1)$

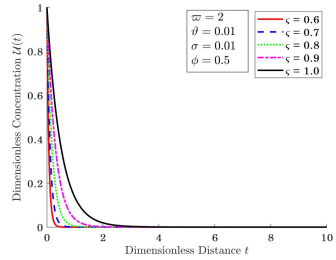

(a) Dimensionless concentration $\mathcal{U}(t)$

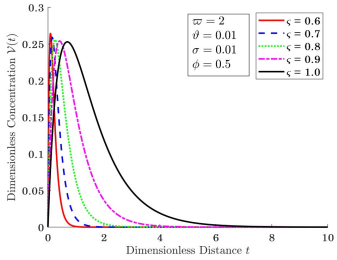

(b) Dimensionless concentration $\mathcal{V}(t)$

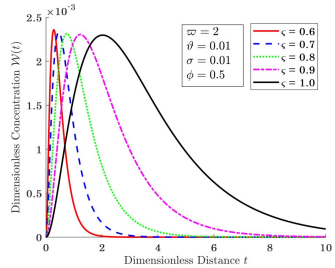

(c) Dimensionless concentration $\mathcal{W}(t)$

Figure 3: Graphical representation of the dimensionless concentrations $\mathcal{U}, \mathcal{V}, \mathcal{W}$ under different dimensionless parameter values and varying fractional orders ς $(0.6 - 1)$

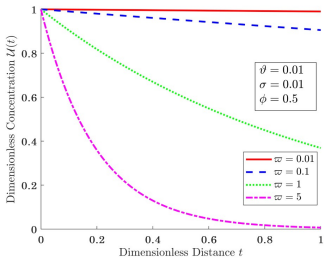

(a) Impact of varying ϖ on $\mathcal{U}(t)$

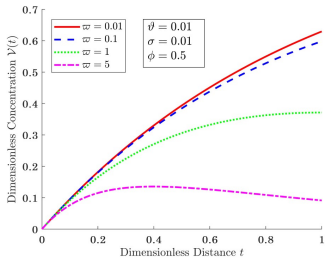

(b) Impact of varying ϖ on $\mathcal{V}(t)$

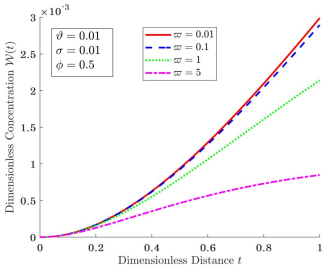

(c) Impact of varying ϖ on $\mathcal{W}(t)$

Figure 4: Graphical representation of the dimensionless concentrations $\mathcal{U}, \mathcal{V}, \mathcal{W}$ under different dimensionless parameter values ϖ and fractional order $\varsigma = 1$

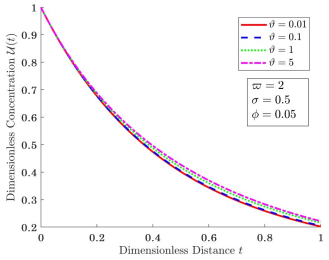

(a) Impact of varying ϑ on $\mathcal{U}(t)$

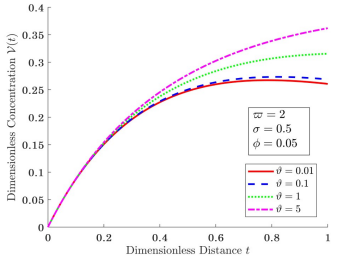

(b) Impact of varying ϑ on $\mathcal{V}(t)$

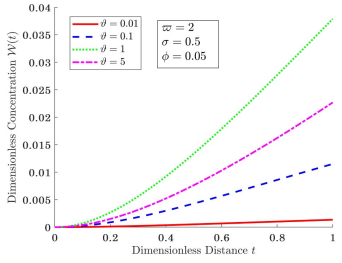

(c) Impact of varying ϑ on $\mathcal{W}(t)$

Figure 5: Graphical representation of the dimensionless concentrations $\mathcal{U}, \mathcal{V}, \mathcal{W}$ under different dimensionless parameter values ϑ and fractional order $\varsigma = 1$

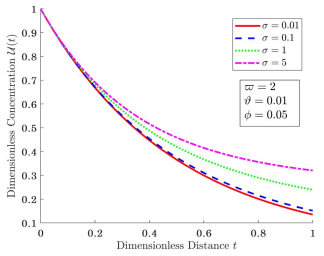

(a) Impact of varying σ on $\mathcal{U}(t)$

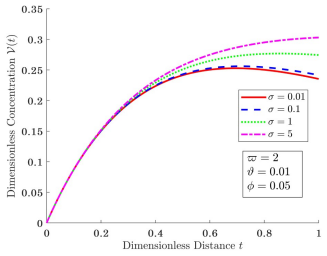

(b) Impact of varying σ on $\mathcal{V}(t)$

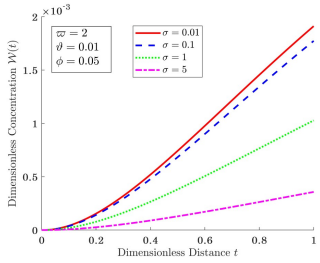

(c) Impact of varying σ on $\mathcal{W}(t)$

Figure 6: Graphical representation of the dimensionless concentrations $\mathcal{U}, \mathcal{V}, \mathcal{W}$ under different dimensionless parameter values σ and fractional order $\varsigma = 1$

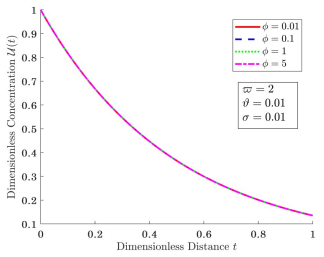

(a) Impact of varying ϕ on $\mathcal{U}(t)$

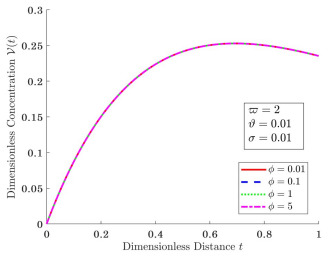

(b) Impact of varying ϕ on $\mathcal{V}(t)$

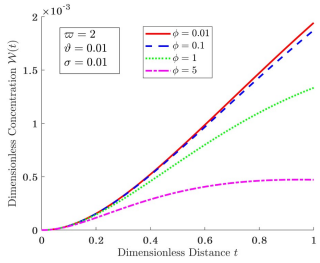

(c) Impact of varying ϕ on $\mathcal{W}(t)$

Figure 7: Graphical representation of the dimensionless concentrations $\mathcal{U}, \mathcal{V}, \mathcal{W}$ under different dimensionless parameter values ϕ and fractional order $\varsigma = 1$

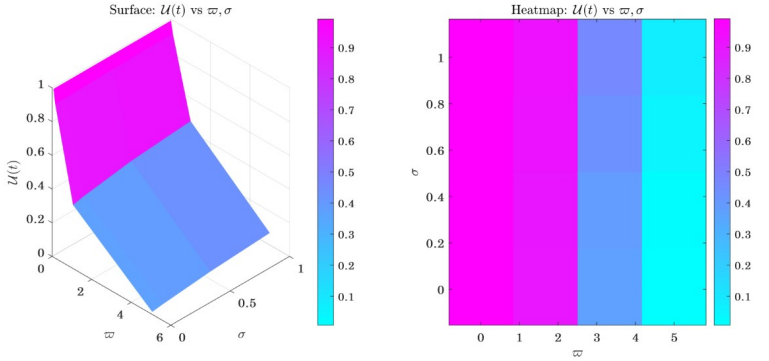

(a) Impact of varying ϖ and σ on $\mathcal{U}(t)$

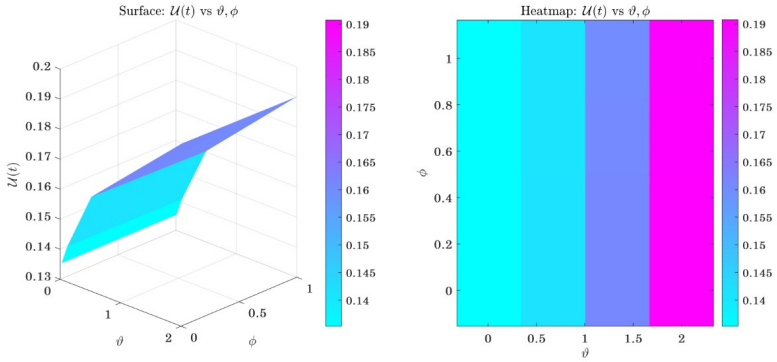

(b) Impact of varying ϑ and ϕ on $\mathcal{U}(t)$

Figure 8: Surface and heatmap representation of the dimensionless concentration $\mathcal{U}(t)$ for different values of the dimensionless parameters ϖ, ϑ, σ, ϕ

6 Conclusion

Although numerous studies have examined enzyme reaction models using classical differential equations, the application of fractional-order derivatives remains limited, particularly for systems involving multiple intermediate complexes. This study presents the first known attempt to model a double-intermediate enzyme-catalyzed reaction using the fractional calculus. A fractional-order mathematical model was formulated within the Caputo derivative framework, transformed into a dimensionless form, and numerically solved using the generalized Euler method.

The numerical simulations conducted in this study revealed that the behavior of the system was highly sensitive to the dimensionless parameters ϖ, ϑ, σ, and ϕ. Specifically, increasing ϖ leads to a reduction in all concentration levels ($\mathcal{U}$, $\mathcal{V}$, and $\mathcal{W}$), indicating that excessively high catalytic efficiency may deplete the reactants too rapidly, destabilizing the system. Therefore, maintaining a moderate value of ϖ is advisable to ensure a controlled enzymatic progression.

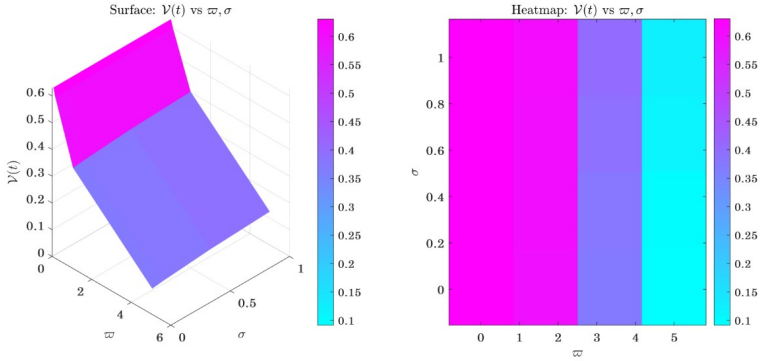

(a) Impact of varying ϖ and σ on $\mathcal{V}(t)$

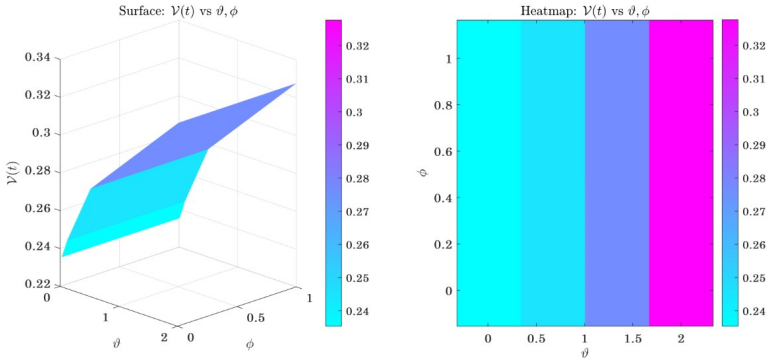

(b) Impact of varying ϑ and ϕ on $\mathcal{V}(t)$

Figure 9: Surface and heatmap representation of the dimensionless concentration $\mathcal{V}(t)$ for different values of the dimensionless parameters ϖ, ϑ, σ, ϕ

Similarly, a high value of ϑ increases all concentrations, suggesting that substrate saturation strongly amplifies the reaction dynamics. However, an excessively high ϑ may lead to over-accumulation of intermediates. By contrast, increasing σ raises $\mathcal{U}$ and $\mathcal{V}$ but reduces $\mathcal{W}$, indicating a trade-off between intermediate complex stability and product formation; thus, minimizing σ can enhance the progression toward product release. Finally, variations in ϕ primarily affect the terminal complex $\mathcal{W}$ with higher values suppressing its accumulation. Hence, reducing ϕ is not recommended if an efficient product formation is desired. Overall, tuning these parameters offers a valuable strategy for modulating enzymatic behavior, and the fractional-order model effectively captures these subtle changes.

This enhanced modeling approach captures subtle dynamic features that are otherwise overlooked in classical models. Overall, this study demonstrates the efficacy of fractional calculus in modeling complex biochemical reactions and provides a foundation for further research. Future

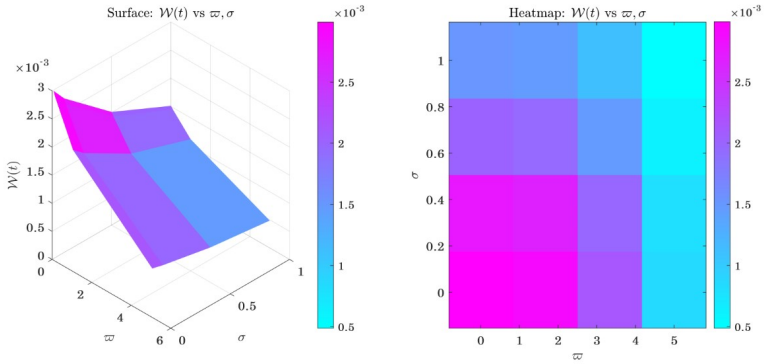

(a) Impact of varying ϖ and σ on $\mathcal{W}(t)$

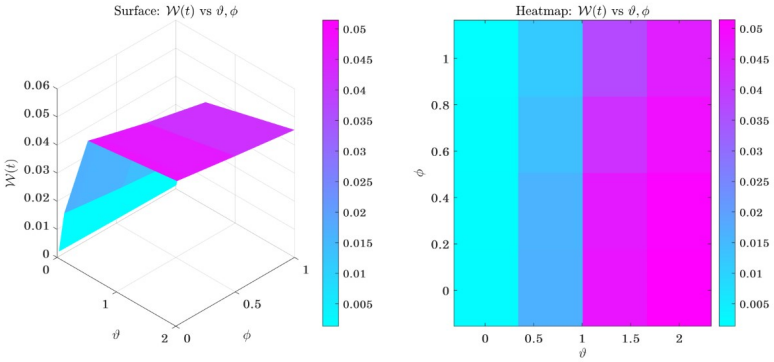

(b) Impact of varying ϑ and ϕ on $\mathcal{W}(t)$

Figure 10: Surface and heatmap representation of the dimensionless concentration $\mathcal{W}(t)$ for different values of the dimensionless parameters ϖ, ϑ, σ, ϕ

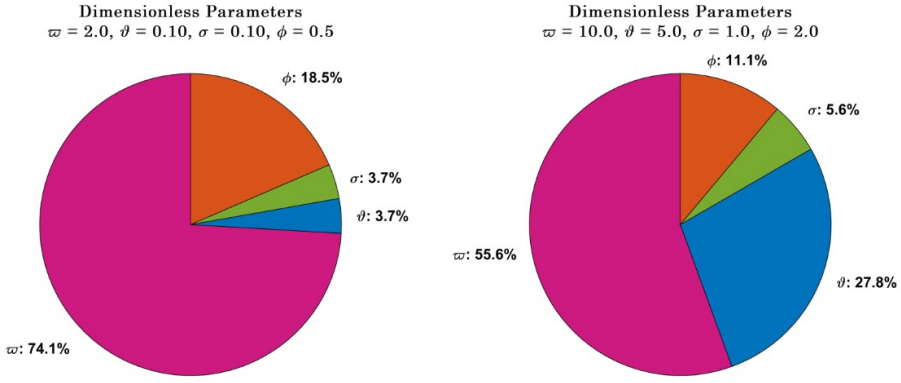

Figure 11: Pie chart representing the sensitivity of the dimensionless parameters ϖ, ϑ, σ, ϕ

research should incorporate machine-learning strategies, parameter estimation techniques, and validation with experimental data to extend the practical applicability of the proposed model.

Acknowledgment

The authors express their sincere gratitude to the anonymous reviewers for their insightful comments, which helped to improve the quality of this manuscript. Also, the author N. Jeeva would like to thank K.S.Rangasamy College of Technology for its continuous support.

Data Availability

All the data generated in this manuscript are included in the list of references.

Conflicts of Interest

The authors declare that they have no conflict of interest associated with the publication of this paper.

Declaration of competing interest

The authors declare that they have no conflicts of interest.

References

[1] Alqhtani, M. and Saad, K.M. *Fractal–fractional Michaelis–Menten enzymatic reaction model via different kernels*, Fractal Fract., 6(1) (2021), 13.

[2] Alqhtani, M., Sadek, L. and Saad, K.M. *The Mittag-Leffler–Caputo–Fabrizio fractional derivative and its numerical approach*, Symmetry, 17(5) (2025), 800.

[3] Chethan, H.B., Turki, N.B. and Prakasha, D.G. *High performance computational approach to study model describing reversible two-step enzymatic reaction with time fractional derivative*, Sci. Rep., 14(1) (2024).

[4] Dharmalingam, K.M., Jeeva, N. and Alessa, N. *Application of Chebyshev Polynomial-Exponential Method and Tamimi-Ansari Method in dengue transmission dynamics: a comparative study*, Int. J. Anal. Appl., 22 (2024), 219.

[5] Frenzen, C.L. and Maini, P.K. *Enzyme kinetics for a two-step enzymic reaction with comparable initial enzyme-substrate ratios*, J. Math. Biol., 26(6) (1988), 689–703.

[6] Haq, I.U., Yavuz, M., Ali, N. and Akgül, A. *A SARS-COV-2 fractional-order mathematical model via the modified Euler method*, Math. Comput. Appl., 27(5) (2022), 82.

[7] Haubold, H.J., Mathai, A.M. and Saxena, R.K. *Mittag-Leffler functions and their applications*, J. Appl. Math., 2011(1) (2011) 1–51.

[8] Ibrahim, M.S., Pavithra, S., Kumar, S.R., Ashokan, R. and Rajendran, L. *Modelling of non linear enzyme reaction process using variational iteration method*, Int. J. Comput. Eng. Res., 6 (2016), 2250–3005.

[9] Jeeva, N. and Dharmalingam, K.M. *Numerical analysis of skin cancer model induced by ultraviolet radiation*, Int. J. Biomathematics, (2024) 2450137.

[10] Jeeva, N. and Dharmalingam, K.M. *Numerical analysis and artificial neural networks for solving nonlinear tuberculosis model in SEITR framework*, Adv. Theory Simul., 8(6) (2025) 2401287.

[11] Khan, F.S., Khalid, M., Bazighifan, O. and El-Mesady, A. *Euler's numerical method on fractional DSEK model under ABC derivative*, Complexity, 2022(1) (2022).

[12] Kim, V.A. and Parovik, R.I. *Application of the explicit Euler method for numerical analysis of a nonlinear fractional oscillation equation*, Fractal Fract., 6(5) (2022), 274.

[13] Koshland, D. *The key-lock theory and the induced fit theory*, Angew. Chem. Int. Ed. Engl., 33 (1995), 2375–2378.

[14] Li, H., Zhang, L., Hu, C., Jiang, Y. and Teng, Z. *Dynamical analysis of a fractional-order predator-prey model incorporating a prey refuge*, J. Appl. Math. Comput., 54(1–2) (2016), 435–449.

[15] Luchko, Y. *Fractional differential equations with the general fractional derivatives of arbitrary order in the Riemann–Liouville sense*, Mathematics, 10(6) (2022), 849.

[16] Manivel, M., Venkatesh, A. and Kumawat, S. *Numerical simulation for the co-infection of Monkeypox and HIV model using fractal-fractional operator*, Model. Earth Syst. Environ., 11(3) (2025) 157.

[17] Manivel, M., Venkatesh, A. and Kumawat, S. *A comprehensive study of monkeypox disease through fractional mathematical modeling*, Math. Model. Numer. Simul. Appl., 5(1) (2025), 65–96.

[18] Manivel, M., Venkatesh, A., Arunkumar, K., Raj, M.P. and Shyamsunder, N. *A mathematical model of the dynamics of the transmission of monkeypox disease using fractional differential equations*, Adv. Theory Simul., 7(9) (2024) 2400330.

[19] Mrope, F. and Jeeva, N. *Modeling the transmission dynamics of banana bunch top disease in banana plants*, Eurasian J. Math. Comput. Appl., 12(3) (2024), 73–90.

[20] Murray, J.D. *Reaction kinetics*, in: Mathematical Biology, Springer, Berlin, Heidelberg, (1989), 109–139.

[21] Nestl, B., Nebel, B. and Hauer, B. *Recent progress in industrial biocatalysis*, Curr. Opin. Chem. Biol., 15 (2010), 187–193.

[22] Radhakrishnan, B., Chandru, P. and Nieto, J.J. *A study of nonlinear fractional-order biochemical reaction model and numerical simulations*, Nonlinear Anal. Model. Control, 29(3) (2024), 588–605.

[23] Reena, A., Raja, R. and Swaminathan, R. *Theoretical analysis of pre-steady state behaviour of non-linear double intermediate enzymatic reaction*, Contemp. Math., (2024), 2565–2584.

[24] Saad, K.M., Abdo, M.S. and Hamanah, W.M. *Existence and controllability analysis of multi-term fractional coupled systems with generalized [ψ, ω]-Caputo-Fabrizio operators*, Sci. Rep., 15(1) (2025) 34434.

[25] Saber, S. and Solouma, E. *The generalized Euler method for analyzing zoonotic disease dynamics in baboon–human populations*, Symmetry, 17(4) (2025), 541.

[26] Saber, S., Solouma, E., Alharb, R.A. and Alalyani, A. *Chaos in fractional-order glucose–insulin models with variable derivatives: insights from the Laplace–Adomian decomposition method and generalized Euler techniques*, Fractal Fract., 9(3) (2025), 149.

[27] Sharmila, D., Praveen, T. and Rajendran, L. *Mathematical modeling and analysis of non-linear enzyme catalyzed reaction processes*, J. Theor. Chem., 2013 (2013), 1–7.

[28] Thangapandi, C., Kuppusamy, R., Muthukumar, S. and Srinivasan, R. *Analytical solutions of non-linear boundary value problem for chemical reactions of enzyme substrate*, Malaya J. Matematik, 1 (2020), 435–444.